Protonation of the Binuclear Metal Center within the Active Site of Phosphotriesterase†

Cynthia R. Samples, Timothy Howard, Frank M. Raushel, and Victoria J. DeRose*

Department of Chemistry, P.O. Box 30012, Texas A&M University, College Station, Texas 77842-3012

Received April 5, 2005; Revised Manuscript Received June 17, 2005

ABSTRACT: Phosphotriesterase (PTE) is a binuclear metalloenzyme that catalyzes the hydrolysis of organophosphates, including pesticides and chemical warfare agents, at rates approaching the diffusion controlled limit. The catalytic mechanism of this enzyme features a bridging solvent molecule that is proposed to initiate nucleophilic attack at the phosphorus center of the substrate. X-band EPR spectroscopy is utilized to investigate the active site of Mn/Mn-substituted PTE. Simulation of the dominant EPR spectrum from the coupled binuclear center of Mn/Mn-PTE requires slightly rhombic zero-field splitting parameters. Assuming that the signal arises from the $S = 2$ manifold, an exchange coupling constant of $J = -2.7 \pm 0.2$ cm^{-1} ($H_{ex} = -2JS_1 \cdot S_2$) is calculated. A kinetic pK_a of 7.1 ± 0.1 associated with loss in activity at low pH indicates that a protonation event is responsible for inhibition of catalysis. Analysis of changes in the EPR spectrum as a function of pH provides a pK_a of 7.3 ± 0.1 that is assigned as the protonation of the hydroxyl bridge. From the comparison of kinetic and spectral pK_a values, it is concluded that the loss of catalytic activity at acidic pH results from the protonation of the hydroxide that bridges the binuclear metal center.

Phosphotriesterase (PTE)[1] catalyzes the hydrolysis of a wide range of organophosphate esters, including agricultural pesticides and chemical warfare agents (*1*−*3*). The enzyme has been isolated from soil bacteria, but the natural substrate for PTE is not known. PTE is a member of the amidohydrolase superfamily, which also includes urease, dihydroorotase, and approximately 30 other enzymes of known specificity (*4*). The high-resolution X-ray crystal structure of Zn/Zn-PTE reveals that it is a homodimeric protein containing an active site with two divalent metal ions embedded within a $(\beta/\alpha)_8$-barrel motif (*5*). The α-metal ion is ligated by His-55, His-57, and Asp-301 while the β-metal ion is coordinated to His-201 and His-230 as illustrated in Figure 1. The two metal ions are bridged by a carboxylated Lys-169 and a molecule from solvent that is either hydroxide or water. The α-metal has a ligand coordination number of five and is considered to be more buried within the protein. The β-metal is more solvent exposed and acquires additional water ligands, resulting in penta- or hexacoordination, depending upon the identity of the bound metal (*5*). Both metals are required for full catalytic activity. Zinc is the apparent native metal ion, but substantial catalytic activity is observed with the Co-, Cd-, Mn-, or Ni-substituted forms of the enzyme (*6*). Kinetic studies have shown that the kinetic constants, k_{cat} and k_{cat}/K_m, are dependent upon the identity of the specific metal ions within the active site. The enzymatic hydrolysis of the insecticide paraoxon is presented in Scheme 1.

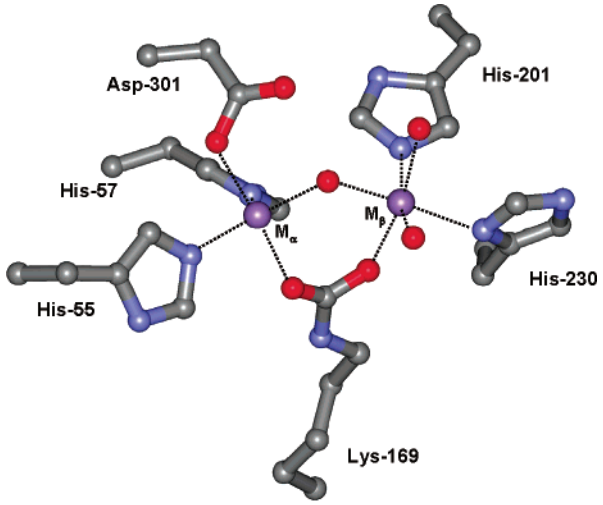

FIGURE 1: Representation of the binuclear metal center within the active site of Mn/Mn-PTE. The manganese ions are depicted as purple spheres. The coordinates were obtained from the PDB entry, 1i0b.

A comprehensive mechanism for the enzymatic hydrolysis of organophosphates by PTE has been proposed (*7*). In this mechanism hydroxide is activated for nucleophilic attack through a hydrogen bonding interaction with Asp-301 and ligation to the binuclear metal center (*8*, *9*). The phosphoryl oxygen bond of the substrate is polarized by a direct

† This work was supported in part by the NIH (GM 33894 to F.M.R.), the NSF (CHE-0111696 to V.J.D. and CHE-0092010 for Texas A&M EPR facilities), and the Robert A. Welch Foundation (A-1314 to V.J.D.).

* To whom correspondence may be addressed. Tel: 979-862-1401. Fax: 979-845-4719. E-mail: derose@mail.chem.tamu.edu.

[1] Abbreviations: PTE, phosphotriesterase; EPR, electron paramagnetic resonance; MES, 2-(*N*-morpholino)ethanesulfonic acid; PIPES, 1,4-piperazinediethanesulfonic acid; HEPES, *N*-(2-hydroxyethyl)piperazine-*N*′-2-ethanesulfonic acid; TAPS, 3-[tris(hydroxymethyl)methyl]-aminopropanesulfonic acid; CHES, 2-(cyclohexylamino)ethanesulfonic acid; TABS, *N*-tris(hydroxymethyl)methyl-4-aminobutanesulfonic acid; TMEDA, *N*,*N*,*N*′,*N*′,-tetramethylethylenediamine; TMTACN, 1,4,7-trimethyl-1,4,7-triazacyclononane.

10.1021/bi0506270 CCC: $30.25
Published on Web 07/29/2005

Scheme 1

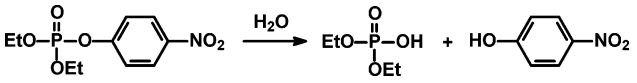

interaction to the β-metal. The phosphotriester bond is cleaved in an S_N2-like reaction that results in the liberation of the leaving-group and the parent diester products. However, the identity of hydroxide as the solvent bridge has not been confirmed by spectroscopic methods.

The pH−rate profile for PTE shows a decrease in catalytic activity as the pH is lowered. The apparent pK_a value for the loss of catalytic activity varies from 5.8 to 8.1, depending upon the identity of the metal ions substituted within the active site (*6*). Since organophosphate substrates for PTE do not ionize in this pH range, the functional group that is protonated with the loss of catalytic activity must originate from the enzyme. The most likely candidates for this protonation site are Asp-301 and the hydroxide that has been proposed to bridge the two divalent cations. Asp-301 is hydrogen bonded to the bridging ligand and additionally coordinated to the α-metal ion. The mutation of Asp-301 to an alanine or asparagine results in the loss of substantial catalytic activity but does not significantly change the value of the kinetic pK_a (*7*).

Electron paramagnetic resonance (EPR) spectroscopy can be used to obtain unique structural and mechanistic information about metal centers within enzyme active sites. For example, with Mn(II)-containing enzymes, EPR spectroscopy has been used to investigate inhibitor binding, metal−metal interactions, metal−metal exchange coupling, and the identity of metal−metal bridging ligands (*10*−*13*). EPR has also been used to study metal−protein interactions and substrate binding orientations for non-manganese enzymes, such as ribonucleotide reductase and enolase, via substitution of the native metal ions with manganese (*14*, *15*). Prior EPR investigations of Mn/Mn- and Cu/Cu-substituted PTE established that the structure of the metal center is binuclear in an asymmetric nitrogen and oxygen coordination environment (*16*, *17*).

This paper probes the identity of the solvent bridging species by monitoring perturbations in the EPR spectrum of Mn/Mn-PTE resulting from changes in pH. The EPR spectrum of Mn/Mn-PTE was also simulated, showing its origin from a spin-coupled system with slight rhombicity. The identity of the protonated species responsible for the loss in the catalytic activity of PTE was addressed via a direct comparison of the effect of pH on the kinetic constants and EPR spectra. From these studies, the solvent bridge between the two divalent cations is postulated as hydroxide and the diminution of catalytic activity at low pH is proposed to be due to the loss of the bridging nucleophile.

MATERIALS AND METHODS

Materials. Diethyl-*p*-nitrophenylphosphate (paraoxon) and all buffers were purchased from Sigma except for *N*-(2-hydroxyethyl)piperazine-*N*′-2-ethanesulfonic acid (HEPES), which was purchased from United States Biochemical. Bacterial cell growth protocols, enzyme purification, preparation of apo-enzyme, and the reconstitution of PTE with manganese were performed as previously described (*6*, *16*).

Kinetic Measurements. The values of k_{cat} and k_{cat}/K_m for Mn/Mn-PTE were determined by measuring the change in absorbance at 347 nm upon hydrolysis of paraoxon (20−2000 μM) to *p*-nitrophenol ($\epsilon_{347} = 5.1 \times 10^4$ M^{-1} cm^{-1}) and diethyl phosphate in 100 mM buffer at 30 °C with a $Spectra_{Max}$ PLUS 384 plate reader from Molecular Devices. The pH was varied from 6.0 to 9.5 in increments of 0.2, and the final pH was measured at the conclusion of the enzymatic reaction. The buffers used for this investigation were MES, pH 5.5−6.4; PIPES, pH 6.5−7.0; HEPES, pH 7.1−8.0; TAPS, pH 8.1−8.9; CHES, pH 9.0; and TABS, pH 9.1−9.5.

Data Analysis. The kinetic constants were obtained by fitting the data to eq 1, where v is the initial velocity, E_t is the enzyme concentration, k_{cat} is the turnover number, K_m is the Michaelis constant, and A is the concentration of substrate. The kinetic pK_a value for Mn/Mn-PTE with paraoxon as the substrate was determined by fitting the pH−rate profile to eq 2, where y is k_{cat}/K_m for the hydrolysis of paraoxon, C is the pH-independent value of y, H is the proton concentration, and K is the dissociation constant for the ionizable species (*18*). The apparent pK_a value determined from the changes in the EPR spectra as a function of pH for Mn/Mn-PTE was also obtained by fitting the data to eq 2, where y is the fraction of the total signal intensity associated with the antiferromagnetically coupled binuclear manganese in the sample.

$$v/E_t = (k_{cat}A)/(K_m + A) \quad (1)$$

$$\log y = \log(C/(1 + (H/K))) \quad (2)$$

EPR Sample Preparation. Mn/Mn-substituted PTE samples of ∼1.0 mg/mL, pH 8.0, were concentrated to ∼12 mg/mL using a YM-10 Centricon microconcentrator from Amicon. Removal of unbound manganese from the protein sample was accomplished by elution through a PD-10 Sephadex G-25 desalting column from Amersham. Changes in pH were achieved by exchange of the protein into 100 mM buffer at the desired pH using a PD-10 column. Samples used to observe the recovery of the binuclear signal at high pH following incubation at low pH were not treated with a PD-10 column in order to minimize loss of labile Mn(II). These samples were diluted into concentrated buffer to achieve the desired pH. All EPR samples were initially frozen in liquid nitrogen at a concentration of 200 μM PTE containing 30% (v/v) glycerol. The protein concentrations were determined by measuring the absorbance at 280 nm using an extinction coefficient of 29 300 M^{-1} cm^{-1} (*6*). The metal content was determined using furnace atomic absorption spectroscopy with a Perkin-Elmer AAnalyst 700. Mn(II) spin quantitation was determined by double integration of the derivative spectrum and comparison with standards of $MnCl_2$ at known concentration. The spin concentrations determined by double integration of the EPR signals matched the metal concentration in the samples predicted by atomic absorption.

EPR Spectroscopy. X-band EPR measurements were obtained using a Bruker ESP 300 spectrometer with a TE_{102} cavity, an Oxford Instruments liquid helium cryostat, an HP 5352B microwave frequency counter, and a Bruker ER 041XG microwave bridge. The magnetic field modulation amplitude was 20 G at a frequency of 100 kHz. EPR spectra

were obtained at 10 K under nonsaturating power conditions of 2 mW.

Simulation of EPR Spectra. The exchange coupling constant, *J*, of Mn/Mn-PTE was determined by comparing the temperature dependence of the EPR signals to the predicted Boltzmann populations of spin states in an exchange coupled $S_i = S_j = {}^5/_2$ system (*16*). The dominant hyperfine-split signal used for determination of *J* is assumed to arise from the $S = 2$ state of the coupled system. This assumption is based on the inspection of temperature-dependent EPR spectra obtained over the range of 4−20 K, which show that a broad signal assumed to be from the $S = 1$ state is observed at the lowest temperatures, and this signal diminishes with increasing temperature along with appearance of the hyperfine-split signal that is assumed to arise from the $S = 2$ state. Boltzmann populations of individual states, *S*, were calculated using eq 3. EPR spectra of Mn/Mn-PTE were simulated with a FORTRAN 99 computer program, DDPOWJHE, running on an SGI Origin 2000 computer as previously described (*19*). The program diagonalizes the full spin Hamiltonian for an exchange-coupled system using eq 4 and calculates transition probabilities at each magnetic field using Fermi's golden rule. The terms in eq 4 correspond to isotropic exchange coupling, dipolar exchange coupling, single-ion zero-field splitting, electronic and nuclear Zeeman splitting, and hyperfine coupling, respectively. The program contains a temperature-dependent Boltzmann weighting factor, a general line broadening feature, and the ability to limit the number of transitions being simulated (*19*).

$$\text{population}_S = \frac{(2S+1)\exp([-2J(S(S+1) - S_i(S_i+1) - S_j(S_j+1))]/kT)}{\sum_S (2S+1)\exp([-2J(S(S+1) - S_i(S_i+1) - S_j(S_j+1))]/kT)} \quad (3)$$

$$\hat{H} = -2JS_1\cdot S_2 + S_1\cdot\hat{D}\cdot S_2 + \sum_{i=1}^{2}[S_i\cdot\hat{D}_i\cdot S_i + \beta_e\cdot\hat{g}\cdot S_i + \beta_n\cdot\hat{g}_n\cdot I_i + S_i\cdot\hat{A}_i\cdot I_i] \quad (4)$$

RESULTS

EPR Spectral Simulation for Mn/Mn-PTE. The EPR spectrum of Mn/Mn-PTE obtained at 10 K is complex and consists of more than 26 lines with hyperfine splittings of 45 G (Figure 2B). Splittings of 45 G near $g = 2$ are indicative of spin-coupled binuclear Mn(II) centers (*12*, *15*, *19*, *20*). EPR spectra from binuclear centers are distinctly different from uncoupled, mononuclear Mn(II) EPR spectra, which usually consist of a six line pattern at $g = 2$ with hyperfine splittings of around 90 G. The EPR spectra of exchange-coupled Mn/Mn-binuclear centers arise from a temperature-dependent population of multiple spin states, *S*. We attempted to describe the Mn/Mn-PTE spectrum using a simulation routine previously used for the symmetrical binuclear complex of $(Mn)_2(H_2O)(OAc)_4(tmeda)_2$ (*19*).

When the isotropic exchange coupling constant, *J*, has a magnitude larger than the Zeeman energy for a dimanganese(II) system, a spin ladder is defined where *S* is the system's total spin with allowed values given by $S = |S_i + S_j|, |S_i + S_j - 1|, \ldots, |S_i - S_j|$. Each of these states can be treated independently if *J* is the dominant term in the Hamiltonian (*21*). In this case a new Hamiltonian can be defined by eq 5 where D_S and E_S are the zero field splitting parameters for the exchange coupled pair. Figure 3 shows the spin ladder defined by the total spin *S* (only the $S = 0$, 1, and 2 levels are shown), along with the effect of the zero-field splitting parameters *D* and *E* and the allowed EPR transitions within each spin level.

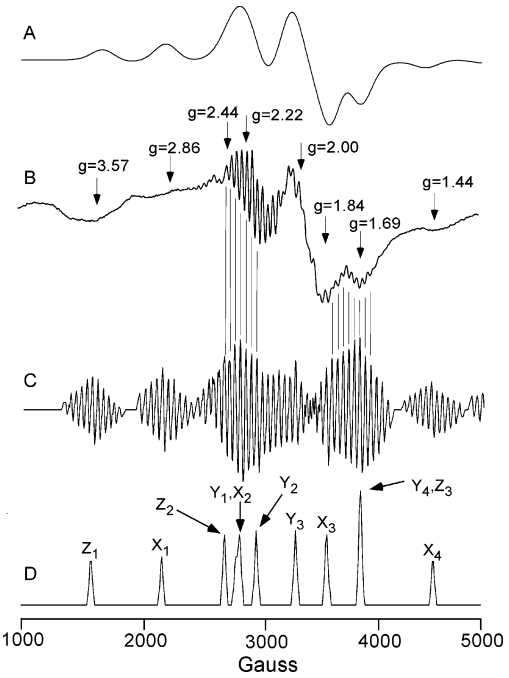

FIGURE 2: Comparison of the X-band EPR signal of PTE to simulations of the $S = 2$ state of a coupled Mn(II) system. Simulation parameters: $g = 2.01$, $D_2 = -0.055$ cm^{-1}, $E_2 = -0.0067$ cm^{-1}. (A) Full powder pattern simulation, $A = 0$, line width = 300 MHz. (B) Mn(II) PTE experimental spectrum at 10 K. (C) Simulation including hyperfine coupling in principal directions only, $A(^{55}Mn) = 272$ MHz, line width = 60 MHz. (D) Simulated principal directions only, $A = 0$, line width = 40 MHz.

$$\hat{H} = -2J[S(S+1) - S_i(S_i+1) - S_j(S_j+1)] + \beta B\cdot\hat{g}\cdot S + D_S[S_z^2 - (1/3)S(S+1)] + E_S(S_x^2 - S_y^2) + (1/2)S\cdot\hat{A}\cdot(I_i + I_j) \quad (5)$$

Equation 5 was used to calculate transition frequencies and probabilities in order to model the experimental EPR spectra of Mn/Mn-PTE.

Previous work with the symmetric compound $(Mn)_2(H_2O)(OAc)_4(tmeda)_2$ demonstrated that the dominant hyperfine-split EPR signal in that binuclear Mn(II) center arises from the $S = 2$ state of the spin ladder. The EPR signal from the $S = 1$ state, populated at lower temperatures, appears as a broad featureless spectrum (*19*). Careful inspection of temperature-dependent data for PTE also reveals a broad spectrum present at 4 K (the lowest temperature used in this study) that is reduced in intensity with increasing temperature, while the distinctive hyperfine-split signal appears with increasing temperature (see Supporting Information). Based on this observation and comparison with previous work, the signal of Figure 2B is assigned to the $S = 2$ state of the PTE spin ladder. Fitting the temperature dependence of this signal to eq 3 gives a value of $J = -2.7 \pm 0.2$ cm^{-1} ($H_{ex} =$

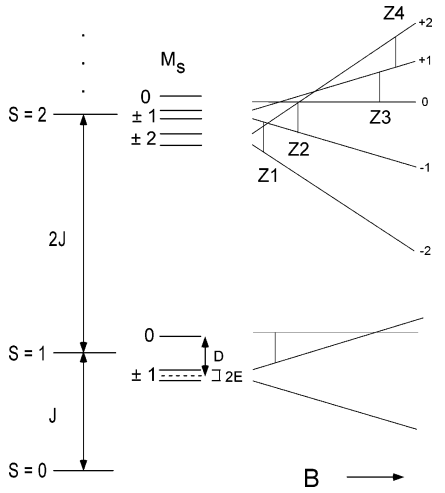

FIGURE 3: Spin ladder produced by exchange coupling between 2 Mn(II) $S = 5/2$ ions. The Zeeman levels and the four $\Delta M_S = 1$ transitions for the $S = 2$ level of the coupled manganese cluster are shown, assuming $D < 0$ and $E < 0$.

$-2JS_1 \cdot S_2$). This differs from a previous result of $J = -5$ cm^{-1}, which was based on the assumption that the signal arises from the $S = 1$ state (*16*).

Two parameters, D and E, are used to describe the zero-field splitting. Unlike the case for the symmetric compound $(Mn)_2(H_2O)(OAc)_4(tmeda)_2$, the PTE spectra could not be simulated by a model in which the two Mn ions are identical and have axial symmetry ($E = 0$). This is not surprising, since the protein crystal structure of PTE shows asymmetry of the two metal sites. In terms of the principal axis directions X, Y, and Z the parameters D and E are defined in eq 6. The signs of D and E are assumed to be negative (*22*).

$$D = -(3/2)D_z, \quad E = -(1/2)(D_x - D_y) \tag{6}$$

Because of the complexity of the Mn/Mn PTE EPR spectrum and the number of parameters in eq 5, a simplified strategy was employed to model the main features of the spectrum in Figure 2B. In the first step, the broad underlying line shape was simulated by using eq 5, but the ^{55}Mn hyperfine interaction term A was set to zero and a line-broadening function added. This simulation produces a full powder spectrum and allows the values for g, D, and E to be estimated. In this step, it was clear that a nonzero value for E was required to reproduce the dominant underlying line shape of the Mn/Mn PTE spectrum. A reasonable fit to the broad features of the PTE spectrum was obtained using the parameters $g = 2.01$, $D_2 = -0.055$ cm^{-1}, $E_2 = -0.0067$ cm^{-1}, $A = 0$, and line width = 600 MHz (Figure 2A). In the next step, the ^{55}Mn hyperfine splittings are added, but for simplicity the simulation is performed only for the three principal orientations along X, Y, and Z. This simulation, shown in Figure 2C, includes hyperfine splittings with $A(^{55}Mn) = 272$ MHz and line width = 60 MHz and illustrates the origin of some of the complex hyperfine splitting observed in the Mn/Mn PTE EPR spectrum. The simulation is further broken down into just the principal transitions in Figure 2D. Each peak in Figure 2D corresponds to one transition between M_s states from the $S = 2$ level as shown for the Z orientation in Figure 3.

Combining the information from simulations C and D, some prominent features of the Mn/Mn PTE EPR spectrum can be assigned. The main pattern of >11 resolved lines centered at $g = 2.22$ likely arises from overlapping transitions Y1 and X2, whereas the lower amplitude but resolved hyperfine pattern at $g = 1.69$ has contributions from transitions Y4 and Z3. The "outer" transitions (including $M_s \pm 2$ sublevels) contribute to broadened peaks at higher and lower g-values. As was observed previously in the case of $(Mn)_2(H_2O)(OAc)_4(tmeda)_2$, these outer transitions are broadened by a mechanism(s) whose origin is not accounted for in these simulations.

The simulations of Figure 2 aid in illustrating the origin of the dominant EPR spectral features from this spin-coupled binuclear Mn(II) system. These features report on the active site of PTE, in particular on the asymmetry of the local coordination environments of the individual Mn(II) ions through the inclusion of a nonzero value for E. Changes in the active site of Mn/Mn PTE are expected to be reflected in D and E, which would change the overall line shape of the EPR spectrum, and also in the exchange coupling J, which would alter the temperature dependence of the spectrum.

There have been recent thorough investigations into this class of EPR spectra based on studies of binuclear Mn(II) model compounds. These simulations take into account the simultaneous population of multiple S levels at a given temperature (*20*, *50*), use multifrequency EPR data (*20*), and discuss broadening mechanisms in terms of microheterogeneity in Mn−Mn distances, among other sources (*20*). An interesting outcome from these studies is that the distinctive hyperfine splittings such as those observed in Mn/Mn PTE are not always observed, or may be observed from higher states such as $S = 3$ (*20*). As described above, the assignment here that the hyperfine-split Mn/Mn PTE signals arise from the $S = 2$ state is made based on inspection of temperature-dependent EPR spectra and experience from a prior model compound study, where J was validated by magnetic susceptibility (*19*). It should be noted that if this Mn/Mn PTE EPR signal does arise from higher S states, the values of J, D, and E that are reported here are overestimated but the general description of origins of the spectral features, and the pH-dependent data described below, are not affected. Because the hyperfine-split EPR signals are clearly observed, Mn/Mn PTE may be a good biological system to investigate with more thorough temperature-dependent and multifrequency techniques (*20*).

pH−Rate Profile. The kinetic parameters for the catalytic activity of PTE depend on the identity of the metal ions in the active site (*6*). Mn/Mn-substituted PTE is reported to have a k_{cat} of 1800 s^{-1}, a K_m of 80 μM, and a k_{cat}/K_m of 2.2 $\times$ 10^7 M^{-1} s^{-1} for the hydrolysis of paraoxon at pH 9.0 (*6*). The pH−rate profile for the hydrolysis of paraoxon by Mn/Mn-PTE is presented in Figure 4A. A pK_a value of 7.1 $\pm$ 0.1 was determined from a fit of the data for k_{cat}/K_m as a function of pH to eq 2. The data fit well to a model in which only one species is protonated and a loss in catalytic activity is observed with protonation of this species.

pH Dependence of EPR Spectra. Perturbations in the spectral properties of the binuclear metal center within the active site of PTE were correlated with the catalytic power of the enzyme as a function of pH. EPR spectra of Mn/Mn-substituted enzyme were obtained as a function of pH and are presented in Figure 5. At pH 8.3, only the binuclear Mn-

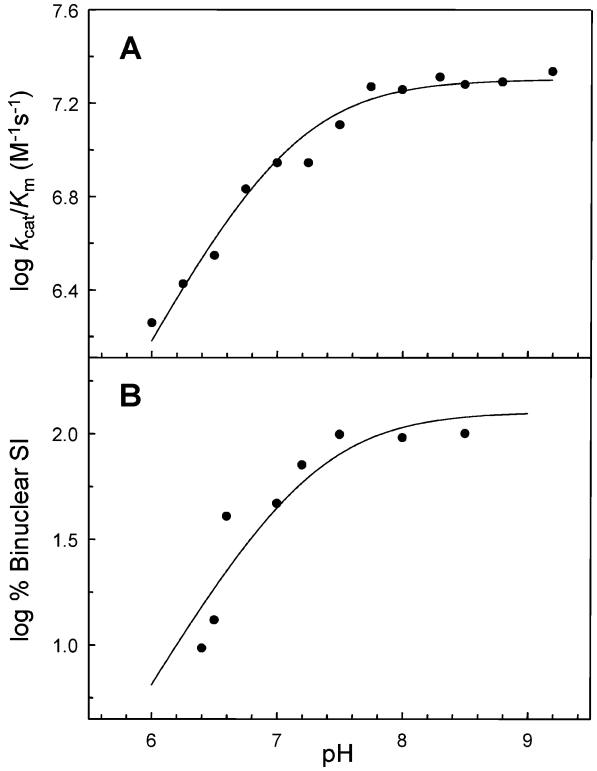

FIGURE 4: The pH profiles for the hydrolysis of paraoxon and the interconversion between the binuclear and mononuclear EPR spectra. (A) The pH−rate profile for the hydrolysis of paraoxon by Mn/Mn-PTE. The experimental data were fit to eq 2 with an apparent kinetic pK_a of 7.1. (B) The pH profile for the titration of the binuclear metal center within the active site of PTE. The experimental data were fit to eq 2 with an apparent pK_a of 7.3. Additional details are provided in the text.

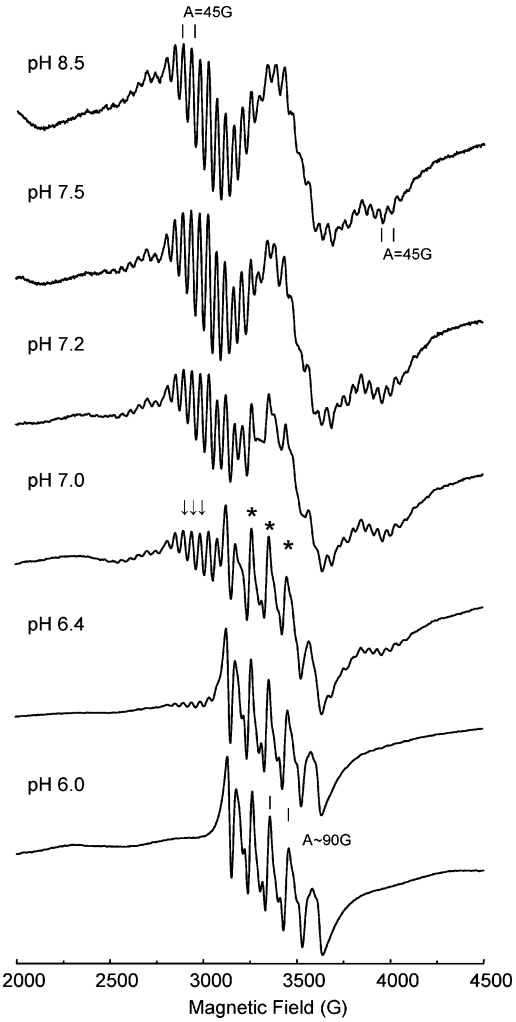

FIGURE 5: X-band EPR spectra of Mn/Mn-PTE at various pH values. Spectra were obtained at 2 mW power, 20 G modulation amplitude, and 10 K. Arrows designate binuclear signal, and asterisks designate mononuclear signal. Additional details are provided in the text.

(II) signal is observed. At pH 7.0, a mononuclear Mn(II) signal is observed at $g = 2$ in addition to the binuclear signal. As the pH decreases, the signal intensity for the coupled binuclear Mn(II) complex diminishes while the signal intensity for mononuclear Mn(II) increases. At pH 6.0, only the mononuclear Mn(II) signal is observed. The signal intensities of three hyperfine splittings from the binuclear Mn/Mn-PTE signal were averaged to quantitate the binuclear Mn/Mn-PTE signal intensity. In Figure 5, the three lines in the EPR spectrum originating from the binuclear Mn/Mn-PTE complex are designated by the thin arrows. The total manganese spin was determined for each spectrum by double integration of the derivative EPR signal. The fraction of the observed spin coupled binuclear signal for each spectrum was determined from the ratio of these measurements. The apparent pK_a associated with the pH-titration of the coupled binuclear metal complex was determined by fitting the log of the fraction of the binuclear signal intensity verses pH to eq 2 and is shown in Figure 4B. The fit of the data resulted in a pK_a value of 7.3 ± 0.1.

The diminution of the signal for the coupled binuclear metal center with decreasing pH can result from the loss of the bridging ligand that enables the exchange coupling between the two metal ions. Alternatively, one or both of the metal ions within the metal center could dissociate from the active site. However, it is unlikely that the mononuclear EPR spectrum observed at low pH originates from Mn(II) that is dissociated from the active site, since a gel filtration procedure was employed that would have separated the macromolecular protein from any loosely bound Mn(II) in solution. It was previously determined that metal binding to the active site of PTE is a cooperative process resulting in two metal ions per active site (*6*). The pH at which catalytic activity is lost depends on the metal identity, but was determined to not be due to loss of metal at the active site (*6*). Therefore, both metals are expected to be present at neutral to low pH. To support this, the reversibility of the effects of pH was confirmed by monitoring the same Mn/Mn PTE sample at pH 8.2, after lowering the pH to 6.8, and again after raising the solution pH to 8.2. Figure 6 illustrates the EPR spectrum of the enzyme before and after the change in pH. After increasing the pH to 8.2, almost complete recovery of the binuclear signal was achieved. The samples subjected to incubation at lower and then higher pH do show some remaining mononuclear Mn(II). This may be due to some adventitious Mn(II) from damaged samples; unlike the case for the EPR samples used for the spectra shown in Figure 5, the samples used to demonstrate reversibility, Figure 6, were not eluted through a desalting column. It is also possible that samples brought back to high pH were not fully equilibrated before freezing, leaving some samples that lack the bridging ligand. Despite the small fraction of

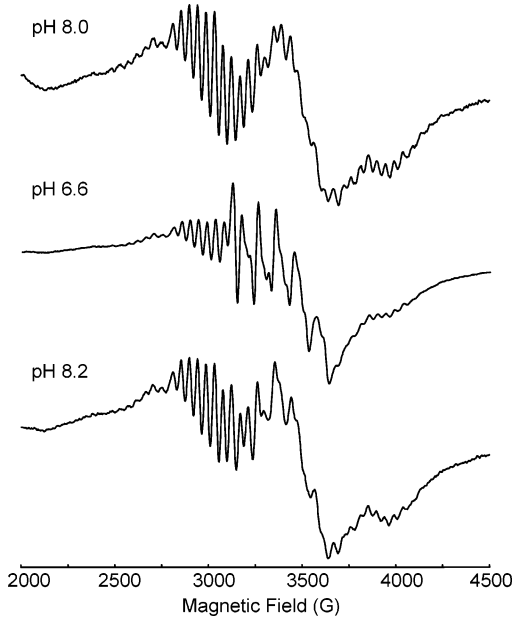

FIGURE 6: X-band spectra of a sample of Mn(II) PTE at pH 8.0, lowered to pH 6.8, and raised to pH 8.2. EPR conditions are 2 mW power, 20 G modulation amplitude, and 10 K.

unrecovered binuclear signal, the restoration of the majority of this signal indicates that formation of the binuclear Mn species is dependent upon and reversible with pH. The ability to recover the binuclear signal requires both metals to be positioned in the active site and available for exchange coupling. Therefore, the effect of pH on the binuclear signal is due to the influence of pH on the protonation state of the bridging ligand which facilitates the exchange coupling between the two metals.

In order to check for weak population of the source of the mononuclear Mn(II) signal in samples subjected to high and low pH conditions, the strong temperature dependence of the overlapping binuclear signal was utilized to diminish its population in the $g = 2$ region. The binuclear signal is temperature dependent with the greatest signal intensity at 10 K. Spectra were collected at temperatures of 3.6 K to 200 K (see Supporting Information). For samples below pH 7.3, the six-line pattern of the mononuclear signal was more pronounced at higher temperatures while the binuclear signal diminished in intensity (see Supporting Information). The binuclear signal in samples above pH 7.3 diminished with increasing temperature, but no mononuclear signal was observed.

DISCUSSION

Spectral Simulation of Mn/Mn-PTE Originating from the $S = 2$ Manifold. The X-band EPR spectrum of PTE resembles that of other enzymes that contain binuclear Mn(II) centers. The spectroscopic signal has a complex line shape, and some of the transitions near $g = 2$ have resolved splittings of 45 G (*12*, *15*, *23*, *24*). Computational simulations of these signals can provide structural information about the active sites containing binuclear metal centers (*20*, *23*). Most simulations of coupled Mn(II) systems have been performed on axially or near axially symmetric complexes requiring only the use of the axial zero-field splitting parameter, *D*, to provide adequate fits to the experimental data. This assumption is inadequate to simulate the EPR signal for PTE. In the case of phosphotriesterase it is known from both X-ray crystallographic and ^{113}Cd NMR studies that the two metal ions occupy distinct chemical environments giving less than axial symmetry (*5*, *25*). From these data it is not surprising that both *D* and *E* would need to be included to accurately simulate the EPR spectrum of PTE. The *D* and *E* values determined from the Mn/Mn-PTE spectrum are -0.055 cm^{-1} and -0.0067 cm^{-1}, respectively. A *D* value of -0.056 cm^{-1} has been reported for the binuclear metal site in arginase where the metal coordination includes both five and six ligands (*23*).

Identification of Hydroxide Bridge. The identity of the bridging species within the binuclear metal center of PTE is of significant interest due to its pivotal role as the species responsible for the nucleophilic attack on the substrate. Metalloproteins containing binuclear metal sites coupled by bridging oxo, hydroxide, and water ligands are not uncommon. PTE, urease, enolase, purple acid phosphatase, methane monooxygenase, Mn-catalase and ribonucleotide reductase are well-characterized examples of these metalloproteins (*5*, *26*−*32*). When the metal center is paramagnetic, the magnetic properties can provide structural information on the identity of the bridging ligand. Magnetic coupling of metal centers is often facilitated by their bridging ligands through a superexchange mechanism. The sign and magnitude of the exchange coupling constant, *J*, are influenced by the bridge identity, metal identity, terminal ligand identity, metal−bridge−metal angle, metal−metal distance, metal−bridge distance, and in-plane bridge−metal alignment (*33*−*38*).

Structural and spectroscopic properties of model complexes with bridging oxygen ligands can aid in understanding the identity of the bridging ligand in PTE. The strength of the exchange interaction generally varies with the protonation state of the bridging oxygen as $O^{-2} > OH^- > OH_2$ (*39*−*42*). Calculating the *J*-value of Mn/Mn PTE using the $S = 2$ manifold, the exchange coupling at the metal center is $J = -2.7 \pm 0.02$ cm^{-1} ($H_{ex} = -2JS_1 \cdot S_2$). Exchange coupling constants observed for dimanganese(II) complexes with a hydroxide bridge range from -2.5 cm^{-1} for a complex with no other bridging species to -9 cm^{-1} for complexes with two additional carboxylate bridges (*23*, *40*). The *J*-value of -2.7 ± 0.02 cm^{-1} is reasonable for a dimanganese(II) complex with a hydroxide bridge and one carboxylate bridge. The metal−bridge distances determined for the X-ray crystal structure for Mn/Mn-PTE are 2.0 and 2.1 Å for the α- and *β*-metal ions, respectively. The reported average distance of 2.0 Å for Mn(II)-μOH$^-$ and 2.5 Å for a Mn(II)-μOH$_2$ model complexes are supportive of a hydroxide bridge for the binuclear metal center in the active site of PTE (*10*, *23*, *40*).

In order to further investigate the identity of the bridging solvent in PTE, EPR was used to evaluate changes within the metal center due to changes in pH. From kinetic measurements it is concluded that the loss in catalytic activity occurs upon protonation of a single species. The pK_a associated with this site is influenced by the identity of the metal ions bound to the active site of PTE (*6*). Four potential models for protonation sites and their consequences are presented in Figure 7. If protonation of the binuclear metal center occurs without the loss of the bridging species, as shown in Figures 7A and 7B, the exchange coupling constant, *J*, would be expected to decrease and increase in magnitude, respectively. In Figure 7A, protonation of the hydroxide

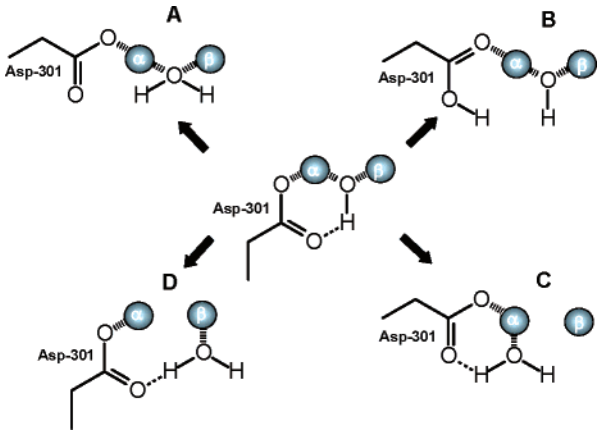

FIGURE 7: Models for the pH dependence of PTE catalytic activity. The active form of PTE is placed in the center, and protonation of the bridging hydroxide or Asp-301 is considered. (A) Bridging water. (B) Protonated Asp-301. (C) Water ligation on the α-metal. (D) Water ligation on the *β*-metal.

bridge would result in a shift of electron density from the bridging oxygen−metal bonds to the new oxygen−hydrogen bond, resulting in a decrease in exchange coupling. In Figure 7B, protonation of Asp-301 would disrupt the hydrogen bonding interaction between the oxygen of Asp-301 and the hydrogen of the hydroxide bridge. This interaction would increase the electron density on the oxygen of the hydroxide bridge and result in an increase in exchange coupling. Changes in *J* would be revealed as changes in the temperature dependence of the binuclear Mn(II) EPR signal. No binuclear signal was observed, over a range of temperatures, for samples poised below pH 6.4 (data not shown). Instead, only a mononuclear Mn(II) signal was observed at these pH values. Due to the absence of the binuclear signal, the models presented in Figures 7A and 7B are ruled out. The absence of a binuclear signal at low pH indicates the loss of the bridging species due to the protonation of the proposed hydroxide bridge. Water ligation could occur to either the α- or *β*-metal, as presented in Figures 7C and 7D, respectively. The ability to regain the binuclear signal after raising the pH supports the reversible protonation of the hydroxide bridge.

The EPR signals from Mn/Mn PTE at low pH values resemble those from mononuclear Mn(II), and yet the ability to recover the binuclear signal upon raising the pH suggests that the Mn(II) ions remain in the PTE active site and in close proximity. The loss of binuclear signal at pH values of 7.25 and lower is not attributed to protonation at the carboxylated lysine since the pK_a of a carboxylate-oxygen ligating a metal would be less than 4. Exchange coupling through this remaining bridge is expected to be minimal, however, due to the high negative electron density on the metal ligating oxygens (*43*). There are few EPR studies of singly bridged dimanganese(II) compounds. The active site of xylose isomerase contains two divalent metal ions that are bridged by a single carboxylate group. In the investigation of xylose isomerase from *Streptomyces rubiginosus* by Witzel and co-workers, the EPR spectra for the $Mn(II)_2$-substituted enzyme showed no evidence of exchange coupling (*44*). In an effort to model dinuclear metal sites containing a single carboxylate bridge, Sakiyama and co-workers synthesized a dimanganese(II) center with each metal ligated by five nitrogens and the oxygen of the bridging acetate (*45*). Weak antiferromagnetic coupling was observed via magnetic susceptibility with a coupling constant of -0.37 cm^{-1}. The EPR spectrum of the compound at 4 K showed a broad line centered at $g = 1.96$ and smaller features at lower and high fields. As an example of another weakly coupled system, weak ferromagnetic exchange coupling of 0.33 cm^{-1} was determined for the dichloro-bridged manganese(II) complex, $[Mn(\mu\text{-}Cl)(2,2'\text{-bi-imidazoline})_2]_2Cl_2$ (*46*). In solution this compound exhibited an EPR signal similar to that observed for mononuclear Mn(II) although the integrity of the cluster could not be verified. It is possible that, upon protonation of the Mn/Mn PTE hydroxide bridge at low pH, the Mn(II) ions are retained with very weak or no coupling, giving rise to the signals observed here, and are easily recoupled upon increasing pH.

Molecular simulation studies of the Zn/Zn- and Cd/Cd-substituted forms of the active site within PTE by Krauss et al. and Ornstein et al. have also determined that hydroxide is the most likely species to bridge the binuclear metal center (*47*, *48*). Krauss et al. found that protonation of the bridging hydroxide resulted in water ligation to the *β*-metal position, which is illustrated in Figure 7D (*47*). Kinetic studies have demonstrated that the α-metal has the greatest influence on the pK_a for substrate turnover as a function of pH. A Zn/Cd-PTE hybrid was prepared with Zn and Cd ions in the α- and *β*-metal sites, respectively (*7*, *24*). The kinetic pK_a of the Zn/Cd PTE hybrid most closely resembled the pK_a of the Zn/Zn-substituted enzyme relative to the Cd/Cd-substituted enzyme. The water ligand after protonation of the bridging hydroxide is therefore expected to reside primarily on the α-metal. The present work supports the protonation of the bridging hydroxide to a bound water molecule as indicated in Figures 7C and 7D. The localization of the water molecule on the α-metal is preferred based upon the kinetic properties of the Zn/Cd-hybrid (*7*, *24*).

Molecular simulations by Ornstein and co-workers on the thermodynamics of protonation of the bridging hydroxide for Zn- and Cd-substituted PTE produced pK_a values of 5.1 and 8.4, respectively (*48*). These simulations are comparable to the previously reported experimental kinetic pK_a values of 5.8 for Zn/Zn-PTE and 8.1 for Cd/Cd-PTE (*6*). Thus, the calculations by Ornstein and co-workers also support the proposal that the site of protonation within the binuclear metal center of PTE is the bridging hydroxide. The protonation of this group results in the loss of catalytic activity.

In this investigation pK_a values of $\sim 7.2 \pm 0.1$ were determined for the protonation of the bridging hydroxide with the Mn/Mn-substituted PTE from both kinetic data and EPR spectra as a function of pH. The pK_a values of water bound to simple Mn complexes have values between 10 and 11 (*43*). The pK_a of water is lowered upon metal coordination due to charge delocalization onto the metal center. Water coordination to two manganese ions further decreases the pK_a of water (*43*, *49*−*51*). The pK_a values of 7.1 and 7.3 obtained from the kinetic and EPR data are therefore reasonable values for water coordinated to both metals within the active site of Mn/Mn-PTE.

In the investigation of rat liver arginase by Dismukes and co-workers, an exchange-coupled dimanganese metal center was observed by EPR. The exchange coupling constant for the complex of arginase with borate is -2.0 ± 0.5 cm^{-1}

(*10*). The two metals have unique ligand coordination environments resulting in an asymmetric environment like that observed in PTE. However, the identities of the metal ligands are different, including an additional carboxylate bridge in the active site of arginase. No changes in the EPR signal of Mn/Mn-arginase were observed at pH values as low as 6.3 by Dismukes, Ash, and co-workers (*10*). The bridging molecule from solvent bound to the binuclear metal center for arginase was therefore concluded to be a water ligand. A kinetic pK_a of 7.5 reflecting loss in arginase catalytic activity at low pH was assigned to His-141 (*10*). The pK_a of a solvent molecule bridging two divalent metals is influenced by the electron withdrawing capability of those metals. The addition of a negatively charged carboxylate bridge to the metal center would lessen this electron withdrawing capability. Therefore, it is possible that the additional carboxylate bridge in arginase results in a predominantly aqua species instead of the hydroxyl species found in PTE. The metal-bridging oxygen distance of ~2.4 Å observed in the X-ray crystal structure of arginase also supports a bridging water ligand. These findings greatly differ from the pH-dependent EPR spectrum of PTE that exhibits reversibility and the metal-bridging oxygen distances in PTE that correlate with a bridging hydroxide ligand.

The Mn/Mn-PTE binuclear center exhibits an exchange coupling constant of $J = -2.7 \pm 0.2$ cm^{-1} that is facilitated through a hydroxide bridge. Protonation of the bridging hydroxide results in the loss of the exchange coupling between the two divalent cations and the loss of catalytic activity. The reversible protonation of the bridging hydroxide has an apparent pK_a of 7.3 based upon changes in the EPR spectrum of Mn/Mn-PTE with alterations in pH. The pH−rate profile for the hydrolysis of paraoxon by Mn/Mn-PTE shows the requirement of a single functional group that must be unprotonated with a pK_a of 7.1. The comparable pK_a values are proposed to result from the protonation of the same ionizable species.

ACKNOWLEDGMENT

We thank Dr. Sarah Aubert (Texas A&M University) for helpful discussions and Dr. Joshua Telser (Roosevelt University) for creating the DDPOWJHE program.

SUPPORTING INFORMATION AVAILABLE

EPR spectra of Mn-substituted phosphotriesterase. This material is available free of charge via the Internet at http://pubs.acs.org.

REFERENCES

1. Dumas, D. P., Caldwell, S. R., Wild, J. R., and Raushel, F. M. (1989) Purification and properties of the phosphotriesterase for *Pseudomonas diminuta*, *J. Biol. Chem. 264*, 19659−19665.
2. Donarski, W. J., Dumas, D. P., Heitmeyer, D. P., Lewis, V. E., and Raushel, F. M. (1989) Structure−activity relationships in the hydrolysis of substrates by the phosphotriesterase from *Pseudomonas diminuta*, *Biochemistry 28*, 4650−4655.
3. Li, W.-S., Lum K. T., Chen-Goodspeed, M., Sogorb, M. A., and Raushel, F. M. (2001) Stereoselective detoxification of chiral sarin and soman analogues by phosphotriesterase, *Bioorg. Med. Chem. 9*, 2083−2091.
4. Holm, L., and Sander, C. (1997) *Proteins: Struct., Funct., Genet. 28*, 72−82.
5. Benning, M. M., Shim, H., Raushel, F. M., and Holden, H. M. (2001) High resolution X-ray structures of different metal-substituted forms of phosphotriesterase from *Pseudomonas diminuta*, *Biochemistry 40*, 2712−2722.
6. Omburo, G. A., Kuo, J. M., Mullins, L. S., and Raushel, F. M. (1992) Characterization of the zinc binding site of bacterial phosphotriesterase, *J. Biol. Chem. 267*, 13278−13283.
7. Aubert, S. D., Li, Y., and Raushel, F. M. (2004) Mechanism for the hydrolysis of organophosphates by the bacterial phosphotriesterase, *Biochemistry 43*, 5707−5715.
8. Benning, M. M., Hong, S.-B., Raushel, F. M., and Holden, H. M. (2000) The binding of substrate analogs to phosphotriesterase, *J. Biol. Chem. 275*, 30556−30560.
9. Lewis, V. E., Donarski, W. J., Wild, J. R., and Raushel, F. M. (1988) Mechanism and stereochemical course at phosphorus of the reaction catalyzed by a bacterial phosphotriesterase, *Biochemistry 27*, 1591−1597.
10. Khangulov, S. V., Sossong, T. M., Ash, D. E., and Dismukes, G. C. (1998) L-arginine binding to liver arginase requires proton transfer to gateway residue His141 and coordination of the guanidinium group to the dimanganese (II,II) center, *Biochemistry 37*, 8539−8550.
11. Meier, A. E., Whittaker, M. M., and Whittaker, J. W. (1996) EPR polarization studies on Mn catalase from *Lactobacillus plantarum*, *Biochemistry 35*, 348−360.
12. Antharavally, B. S., Poyner, R. R., and Ludden, P. W. (1998) EPR spectral evidence for a binuclear Mn(II) center in dinitrogenase reductase-activating glycohydrolase from *Rhodospirillum rubrum*, *J. Am. Chem. Soc. 120*, 8897−8898.
13. Kanyo, Z. F., Scolnick, L. R., Ash, D. E., and Christianson, D. W. (1996) Structure of a unique binuclear manganese cluster in arginase, *Nature 383*, 554−557.
14. Pierce, B. S., Elgren, T. E., and Hendrich, M. P. (2003) Mechanistic implications for the formation of the diiron cluster in ribonucleotide reductase provided by quantitative EPR spectroscopy, *J. Am. Chem. Soc. 125*, 8748−8759.
15. Poyner, R. R., Cleland, W. W., and Reed, G. H. (2001) Role of metal ions in catalysis by enolase: an ordered kinetic mechanism for a single substrate enzyme, *Biochemistry 40*, 8009−8017.
16. Chae, M. Y., Omburo, G. A., Lindahl, P. A., and Raushel, F. M. (1993) Antiferromagnetic coupling in the binuclear metal cluster of manganese-substituted phosphotriesterase, *J. Am. Chem. Soc. 115*, 12173−12174.
17. Chae, M. Y., Omburo, G. A., Lindahl, P. A., and Raushel, F. M. (1995) Utilization of copper as a paramagnetic probe for the binuclear metal center of phosphotriesterase, *Arch. Biochem. Biophys. 316*, 765−772.
18. Meister A., Ed. (1982) *Methods in Enzymology*, Vol. 87, pp 390−405, John Wiley & Sons, Inc., New York.
19. Howard, T., Telser, J., and DeRose, V. J. (2000) An electron paramagnetic resonance study of $Mn_2(H_2O)(OAc)_4(tmeda)_2$ (tmeda = *N*,*N*,*N*′,*N*′,-tetramethylethylenediamine): a model of dinuclear manganese enzyme active sites, *Inorg. Chem. 39*, 3379−3385.
20. Golomek, A. P., and Hendrich, M. P. (2003) Quantitative analysis of dinuclear manganese(II) EPR spectra, *J. Magn. Reson. 165*, 33−48.
21. Owen, J. J. (1961) *Appl. Phys. 32*, 213S−215S.
22. Schultz, B. K., Ye, B., Li, X., and Chan, S. I. (1997) Electronic paramagnetic resonance and magnetic properties of model complexes for binuclear active sites in hydrolase enzymes, *Inorg. Chem. 36*, 2617−2622.
23. Khangulov, S. V., Pessiki, P. J., Ash, D. E., and Dismukes, G. C. (1995) Determination of metal ion separation and energies of the three lowest electronic states of dimanganese(II,II) complexes and enzymes: catalase and liver arginase, *Biochemistry 34*, 2015−2025.
24. Markharm, G. D. (1981) Spatial proximity of two divalent metal ions at the active site of s-adenosylmethionine synthetase, *J. Biol. Chem. 256*, 1903−1914.
25. Omburo, G. A., Mullins, L. S., and Raushel, F. M. (1993) Structural characterization of the divalent cation sites of bacterial phosphotriesterase by ^{113}Cd NMR spectroscopy, *Biochemistry 32*, 9148−9155.
26. Khangulov, S. V., Barynin, V. V., Voevodskaya, N. V., and Grebenko, A. I. (1990) ESR spectroscopy of the binuclear cluster of manganese ions in the active center of manganese-catalase from *Thermus thermophilus*, *Biochim. Biophys. Acta 1020*, 305−310.
27. Un, S., Dorlet, P., Voyard, G., Tabares, L. C., and Cortez, N. (2001) High-field EPR characterization of manganese reconstituted superoxide dismutase from *Rhodobacter capsulatus*, *J. Am. Chem. Soc. 123*, 10123−10124.

28. Clark, P. A., and Wilcox, D. E. (1989) Magnetic properties of the nickel enzymes urease, nickel-substituted carboxypeptidase A, and nickel-substituted carbonic anhydrase, *Inorg. Chem. 28*, 1326−1333.
29. Larsen, T. M., Wedekind, J. E., Rayment, I., and Reed, G. H. (1996) A carboxylate oxygen of the substrate bridges the magnesium ions at the active site of enolase: structure of the yeast enzyme complexed with the equilibrium mixture of 2-phosphoglycerate and phosphoenolpyruvate at 1.8Å resolution, *Biochemistry 35*, 4349−4358.
30. Averill, B. A., Davis, J. C., Burman, S., Zirino, T., Sanders-Loehr, J., Loehr, T. M., Sage, J. T., and Debrunner, P. G. (1987) Spectroscopic and magnetic studies of the purple acid phosphatase from bovine spleen, *J. Am. Chem. Soc. 109*, 3760−3767.
31. Fox, B., Hendrich, M. P., Surerus, K. K., Andersson, K. K., Froland, W. A., Lipscomb, J. D., and Munck, E. (1993) Mössbauer, EPR, and ENDOR studies of the hydroxylase and reductase components of methane monooxygenase from *Methylosinus trichosporium* OB3b, *J. Am. Chem. Soc. 115*, 3688−3701.
32. Davydov, R., Kuprin, S., Graslund, A., and Ehrenberg, A. (1994) Electron paramagnetic resonance study of the mixed-valent diiron center in *Escherichia coli* ribonucleotide reductase produced by reduction of radical free protein R2 at 77K, *J. Am. Chem. Soc. 116*, 11120−11128.
33. Wieghardt, K. (1989) The active sties in manganese-containing metalloproteins and inorganic model complexes, *Angew. Chem., Int. Ed. Engl. 28*, 1153−1172.
34. Weihe, H., and Gudel, H. U. (1997) Quantitative interpretation of the goodenough-kanamori rules: a critical analysis, *Inorg. Chem. 36*, 3632−3639.
35. Hotzelmann, R., Wieghardt, K., Florke, U., Haupt, H. J., Weatherburn, D. C., Bonvoisin, J., Blondin, G., and Girerd, J. J. (1992) Spin exchange coupling in asymmetric heterodinuclear complexes containing the μ-oxo-bis(μ-acetato)dimetal core, *J. Am. Chem. Soc. 114*, 1681−1696.
36. Brunold, T. C., Gamelin, D. R., and Solomon, E. I. (2000) Excited-state exchange coupling in bent Mn(III)−O−Mn(III) complexes: dominance of the π/σ superexchange pathway and its possible contributions to the reactivities of binuclear metalloproteins, *J. Am. Chem. Soc. 122*, 8511−8523.
37. Delfs, C. D., and Stranger, R. (2000) Magnetic exchange in $[Mn_2(\mu\text{-}O)_3(tmtacn)_2]^{2+}$: metal−metal bonding or superexchange?, *Inorg. Chem. 39*, 491−495.
38. Reed, G. H., and Markham, G. D. (1984) *Biological Magnetic Resonance*, Vol. 6, Plenum Press, New York.
39. Ruiz, E., Alemany, P., Alvarez, S., and Cano, J. (1997) Structural modeling and magneto-structural correlations for hydroxo-bridged copper(II) binuclear complexes, *Inorg. Chem. 36*, 3683−3688.
40. Bossek, U., Wieghardt, K., Nuber, B., and Weiss, J. (1989) Bioinorganic model complexes for the active-site in manganese containing catalases−the crystal structures of $[L_2Mn^{II}_2(\mu\text{-}OH)(\mu\text{-}O_2CCH_3)_2](PF_6)\cdot CH_3OH$ and $[L'_2Mn^{III}_2(\mu\text{-}O)(\mu\text{-}O_2CCH_3)_2](I_3)I\cdot H_2O$, *Inorg. Chim. Acta 165*, 123−129.
41. Sakiyama, H., Tamaki, H., Kodera, M., Matsumoto, N., and Okawa, H. (1993) Dinuclear manganese (II) complexes of 2,6-bis[2-(dialkylamino)-ethyliminomethyl]-4-methylphenolate(l-)−synthesis, structure, and magnetism, *J. Chem. Soc., Dalton Trans.* 591−595.
42. Caneschi, A., Ferraro, F., Gatteschi, D., Chiaro Melandui, M., Rey, P., and Sessoli, R. (1989) Synthesis, structure, and magnetic properties of a dinuclear manganese (II) complex with one μ-aqua and 2 μ-carboxylato bridges, *Angew. Chem., Int. Ed. Engl. 28*, 1365.
43. Dismukes, G. C. (1996) Manganese enzymes with binuclear active sites, *Chem. Rev. 96*, 2909−2926.
44. Bogumil, R., Kappl, R., Hüttermann, J., Sudfeldt, C., and Witzel, H. (1993) X- and Q-band EPR studies on the two Mn^{2+}-substituted metal-binding sites of D-xylose isomerase, *Eur. J. Biochem. 213*, 1185−1197.
45. Adams, H., Bailey, N. A., Debaecker, N., Fenton, D. E., Kanda, W., Latour, J.-M., Okawa, H., and Sakiyama, H. (1995) A dinuclear (μ-carboxylato)manganese(II) complex derived from a macrocyclic ligand: a structural model for active sites in natural systems, *Angew. Chem., Int. Ed. Engl. 34*, 2535−2537.
46. van Albada, G. A., Mohamadou, A., Driessen, W. L., de Gelder, R., Tanase, S., and Reedijk, J. (2004) A dinuclear Mn(II) chloro-bridged compound with a weak ferromagnetic Mn-Mn interaction. Synthesis, structure, EPR, and magnetism of $[Mn(\mu\text{-}Cl)(2,2'\text{-biimidazoline})_2]_2Cl_2$, *Polyhedron 23*, 2387−2391.
47. Krauss, M. (2001) *Ab initio* structure of the active sties of phosphotriesterase, *J. Chem. Inf. Comput. Sci. 41*, 8−17.
48. Zheng, F., Zhan, C.-G., and Ornstein, R. L. (2002) Theoretical determination of two structural forms of the active site in cadmium-containing phosphotriesterases, *J. Phys. Chem. B 106*, 717−722.
49. Sivaraja, M., Stouch, T. R., and Dismukes, G. C. (1992) Solvent structure around cations determined by ^{1}H ENDOR spectroscopy and molecular dynamics simulation, *J. Am. Chem. Soc. 114*, 9600−9602.
50. Zheng, M., Khangulov, S. V., Dismukes, G. C., and Barynin, V. V. (1994) Electronic structure of dimanganese (II,III) and dimanganese (III,IV) complexes and dimanganese catalase enzyme: a general EPR spectral simulation approach, *Inorg. Chem. 33*, 382−387.
51. Blanchard, S., Blain, G., Riviere, E., Nierlich, M., and Blondin, G. (2003) Temperature dependence of X- and Q-band EPR spectra of the dinuclear manganese(II) complex $[NO_2Bpmp)Mn_2(\mu\text{-}OAc)_2]$: determination of the exchange constant and of the spin parameters for the S=1, 2, and 3 spin states, *Chem. Eur. J. 9*, 4260−4268.

BI0506270